Int. J. Electrochem. Sci., 8 **(2013)** 12062 - 12077

International Journal of ELECTROCHEMICAL SCIENCE
www.electrochemsci.org

Antibiofouling Properties of Sol-Gel Type Polymers for Aluminium Alloys: Biocorrosion Protection Against *Pseudomonas Aeruginosa.*

N. D. Vejar[1a], *M. I. Azocar*[1a], *L. A. Tamayo*[1a], *E. Gonzalez*[1a], *J.Pavez*[1a], *M. Gulppi*[1a], *J.H.Zagal*[1a], *X. Zhou*[2], *F.Santibañez*[1b], *G. E. Thompson*[2], *M. A. Paez*[1a,*].

[1]Departamento de Química de los Materiales, Facultad de Química y Biología, Universidad de Santiago de Chile. Avenida Libertador Bernardo O´Higgins 3363, Casilla 40, Correo 33. Santiago, Chile[a]. Departamento de Física, Facultad de Ciencias, Universidad de Santiago de Chile. Avenida Ecuador 3493, Santiago, Chile[b].
[2]Corrosion and Protection Centre, School of Materials, The University of Manchester, Manchester M13 9PL, England, UK
[*]E-mail: maritza.paez@usach.cl.

Received: 19 July 2013 / *Accepted:* 27 August 2013 / *Published:* 25 September 2013

The antibiofouling ability of three hybrid sol-gel coatings against *P. aeruginosa* for the protection of AA2024-T3 aluminium alloy has been investigated. The polymers were synthesized by mixing tetraethoxysilane (TEOS) with three precursors: (a) triethoxypropylsilane (TEPRS), (b) triethoxypentylsilane (TEPES) and (c) triethoxyoctylsilane (TEOCS). The main difference between the three precursors is the length of the aliphatic chain of one of the substituents. The antibacterial properties of the polymers were examined using viability techniques. The morphology of the polymers was characterized using scanning electron microscopy (SEM). The resistance of the AA2024 alloy coated with the respective polymers to microbiologically influenced corrosion was evaluated by potentiodynamic polarization. The results showed that the polymers possess antibacterial ability against *P. aeruginosa* and that the length of the aliphatic chain of the precursors does not significantly affect this property. Further, the electrochemical measurements revealed that the coatings inhibited microbiologically influenced corrosion in the mixture of *P. aeruginosa* and 0.1 M NaCl, due to the antibacterial properties of the polymers. A correlation between the degree of protection and the length of the aliphatic chain was revealed. Thus, the longer the chain length, the greater the protective effect. The antibiofouling ability resides mainly on the hydrophobic characteristic of polymers and the pH change occurring at the polymer-electrolyte interface when the coated aluminium alloy was immersed in the electrolytes.

Keywords: aluminium, alloy, microbiological corrosion, polymer coatings, antibiofouling.

1. INTRODUCTION

Microorganisms have a strong tendency to colonize on solid surfaces, leading to a complex microbial community, called biofilm, that strongly adheres to the solid surface [1]. Biofilms are detrimental to the underlying metal substrates, causing physical degradation or biodeterioration of the metal [2-5]. This phenomenon is widely recognized as biocorrosion or microbiologically influenced corrosion. Among the many microorganisms which induce the degradation or corrosion of metallic materials, *Pseudomonas* is associated with corrosion of aluminium and its alloys and has been widely studied [6-12]. For decades, aluminium alloys have been protected against corrosion by multilayer coatings, which are prepared using chromate species. These coatings have distinct properties, including excellent adhesion, self-healing ability and antimicrobial properties. However, the disadvantage of the chromate-based processes is their high cost, and with the waste being hazardous to the environment. Given the ecological and environmental issues, recent effort has been focused on developing environmentally benign coatings with antibiofouling properties that prevent bacterial adhesion and biofilm formation. Organic-inorganic hybrid coatings are of great interest because the organic component can impart specific surface functions, such as hydrophobicity and resistance to cracks, while the inorganic counterparts may confer mechanical strength, durability, resistance to impact and adhesion to the metal surface [13-15]. The organic-inorganic hybrid coatings are generally prepared in two ways using the sol-gel process, involving the organic and inorganic groups being joined through stable chemical bonds [16] or the organic component being simply embedded in the inorganic material and vice versa [17]. Recent studies of polymers based on tetraethoxysilane (TEOS) and triethoxyoctylsilane (TEOCS) showed a significant protective effect of the coatings against aqueous corrosion of AA2024 aluminium alloy [18]. Further, although previous studies have shown that some hybrid polymers exhibit antibacterial properties against *P. aeruginosa*, the origin of this property remains unclear. This study evaluates the antibiofouling capabilities of three polymers as well as the biocorrosion resistance that these polymers, as coatings, may provide to AA2024 aluminium alloy. The three hybrid polymers were generated with a common inorganic precursor, tetraethoxysilane (TEOS), and three different organic precursors. The main difference between the organic precursors is the length of the aliphatic chain on one of their substituents, with 3, 5 and 8 carbons respectively, described as follows: triethoxypropylsilane (TEPRS), triethoxypentylsilane (TEPES) and triethoxyoctylsilane (TEOCS).

2. EXPERIMENTAL

2.1 Substrates

An AA2024-T3 aluminium alloy (1 mm thick of nominal composition (wt. %), 0.529 Si, 0.533 Fe, 4.75 Cu, 0.71 Mn, 1.28 Mg, 0.254 Zn, 0.16 Ti and Al-remainder) was provided by the Chilean aerospace company, ENAER. The specimens were mechanically ground sequentially with SiC paper of 400, 800, 1200 and 2400 grit, washed with distilled water and degreased with acetone. The substrates were then etched in 0.01 M KOH for 10 min and dismutted in 20 v% HNO_3 for 1 min [18].

2.2 Synthesis, preparation and characterization of coatings

Tetraethoxysilane (TEOS, Merck > 99%), triethyloctylsilane (TEOCS Merck,> 99%), triethoxypropylsilane (TEPRS, Finetech > 97%) and triethoxypentylsilane (TEPES, Finetech > 95%), HNO_3 69% (Merck, PA) and propanol (Merck, PA) were used in the synthesis of the sol-gel polymers. The tetraethoxysilane (TEOS) and triethoxyoctylsilane (TEOCS) monomers and propanol were mixed in the ratio 1:1:2, and hydrolyzed with 10% v/v HNO_3 to pH 1 to prepare polymer PSG-08. The polymers, PSG-03 and PSG-05 polymers were prepared using the organic monomers triethoxypropylsilane (TEPRS) and triethoxypentylsilane (TEPES) respectively [18]. The polymer coatings were applied to the aluminium alloy substrate by immersion in the hybrid sol for 15 min and then withdrawn at an average rate of 1 mm/s. After removal from the hybrid sol, the coatings were cured at 100ºC for 1 h unless stated otherwise.

The sol-gel polymers were then characterized using FT-IR. The morphology of the sol-gel coatings was examined in an S-4100 Hitachi scanning electron microscope. The degree of hydrophobicity of the polymers was determined by measuring the contact angle when a drop of water (1 mg) was placed on the polymer surface. Further, after various immersion times of the polymer in distilled water, the consequent pH changes in the water were determined. The measurement was performed with the polymers after different curing times.

2.3 Microbiological tests

The metallic specimens were exposed to UV light (15 min per side) in a laminar flow hood in order to be sterilized along with the material used in this experiment. Unless otherwise stated, the culture medium contained bacteriological peptone (9 g/l, 15.55% total nitrogen, 0.023% calcium, 0.013% magnesium, 1.4% sodium, 7.95 g/l alanine, 7.21 g/l arginine, 6.42 g/l aspartic acid, 0.14 g/l Cystine, 9.93 g/l glutamic acid, 20.71 glycine, 0.93 g/l histidine, 1.41 g/l Isoleucine, 3.02 g/l leucine, 3.69 g/l lysine, 0.92 g/l methionine, 11.71 g/l proline, 3.51 g/l serine, 1.9 g/l threonine, 0.09 g/l tryptophan, 0.75 g/l tyrosine, 2.4 valine. amino nitrogen) and 0.1 M NaCl. The gram negative bacterium *P. aeruginosa* (ATCC # 27853, ISP) were inoculated at 10^8 CFU/ml. Colony forming units (CFU) determination was performed following the McFarland method [19]. The aluminium alloy specimens were exposed to a culture medium inoculated with *P. aeruginosa* for periods of 3, 7, 14 and 21 days.

2.4 Antibacterial properties

The antibacterial properties were evaluated by the modified Zapata procedure [20], with 50 µl of the bacterial strain, *P. aeruginosa* (10^6 CFU/ml), seeded on the coated aluminium alloy. After exposure for 16 h, the surviving bacteria were washed with Tween 80 (Sigma) solution and again sown in Mueller Hinton Agar (Difco).

The antibacterial activity was also examined by viability tests performed using confocal microscopy. The bacterial viability kit used, Live / Dead BacLight (L7012-Sigma), consisted of a

mixture of SYTO 9 [21], which has a green fluorescent colour, and propidium iodide (PI), which gives a red fluorescent colour. The SYTO 9 is permeable to the membrane and stains both viable and non-viable bacteria, while PI, which has a high affinity for nucleic acids and preferably dyed the non-viable bacteria. Viable bacteria (green) and dead bacteria (red) can be distinguished under a fluorescent microscope [29]. After exposure to the media inoculated with *P. aeruginosa* (10^8 CFU/ml), the aluminium alloy specimens, with and without the sol-gel coatings, were stained with 0.1 ml of Live/Dead solution for 15 min. The stained samples were examined under a green filter (excitation/ emission wavelength, 420-480 nm / 520/580 nm) or red filter (excitation / emission wavelength 590-800 nm/ 480-550 nm) in a Zeiss LSM 51 microscope.

2.5 Electrochemical measurements

Specimens, after sterilizing with alcohol and washing thoroughly with distilled water, were exposed to UV light for 15 min, and then tagged to leave a 1 cm^2 testing area. A 3-component, thermoregulated electrochemical cell, including a saturated $Hg/HgSO_4$ electrode (SSE) as reference electrode (0.43 V vs SCE), a platinum wire counter electrode and the AA2024 alloy as the working electrode was used. The electrochemical experiments were performed in sterile culture medium and NaCl 0.1M (details given in Section 2.3). The polarization measurements were carried out at a scan rate of 0.2 mV s^{-1}. A potentiostat/galvanostat AUTOLAB PGSTAT30 with NOVA software 1.6 was employed. The potentiodynamic measurements were performed in triplicate to ensure reproducibility

3. RESULTS

3.1 Coating characterization

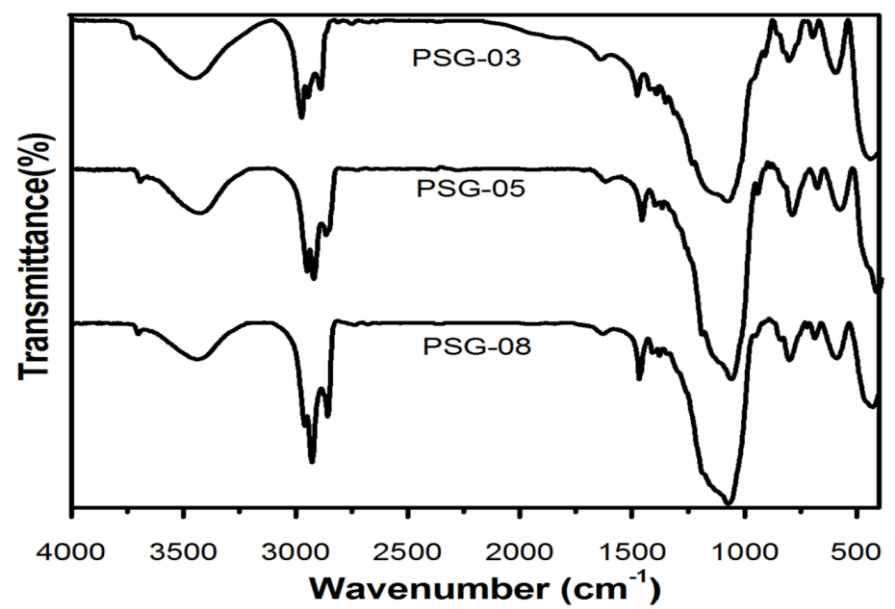

Figure 1. IR spectra of the sol-gel polymers: (a) PSG-03; (b) PSG-05; (c) PSG-08

Figure 1 displays the FT-IR spectra of the resultant sol-gel polymers, showing typical bands that are generally associated with aliphatic substitutions in hybrid polymers at 2959-2962 cm^{-1} ($-CH_3$, asymmetric stretch), 2927-2934 cm^{-1} ($-CH_2$, asymmetric stretch), 2857-2877 cm^{-1} ($-CH_3$ symmetric stretching), 1466-1465 cm^{-1} ($-CH_2$, bending) and 1378-1381 cm^{-1} ($-CH_2$, waging). The bands related to the presence of silica are observed between 1065-1073 cm^{-1} (Si-O-Si, symmetric stretch) and 429-435 cm^{-1} (O-Si-O, bending) [22-24]. It is evident that the intensity of the band corresponding to $-CH_2$ asymmetric stretching increases with increasing aliphatic chain length.

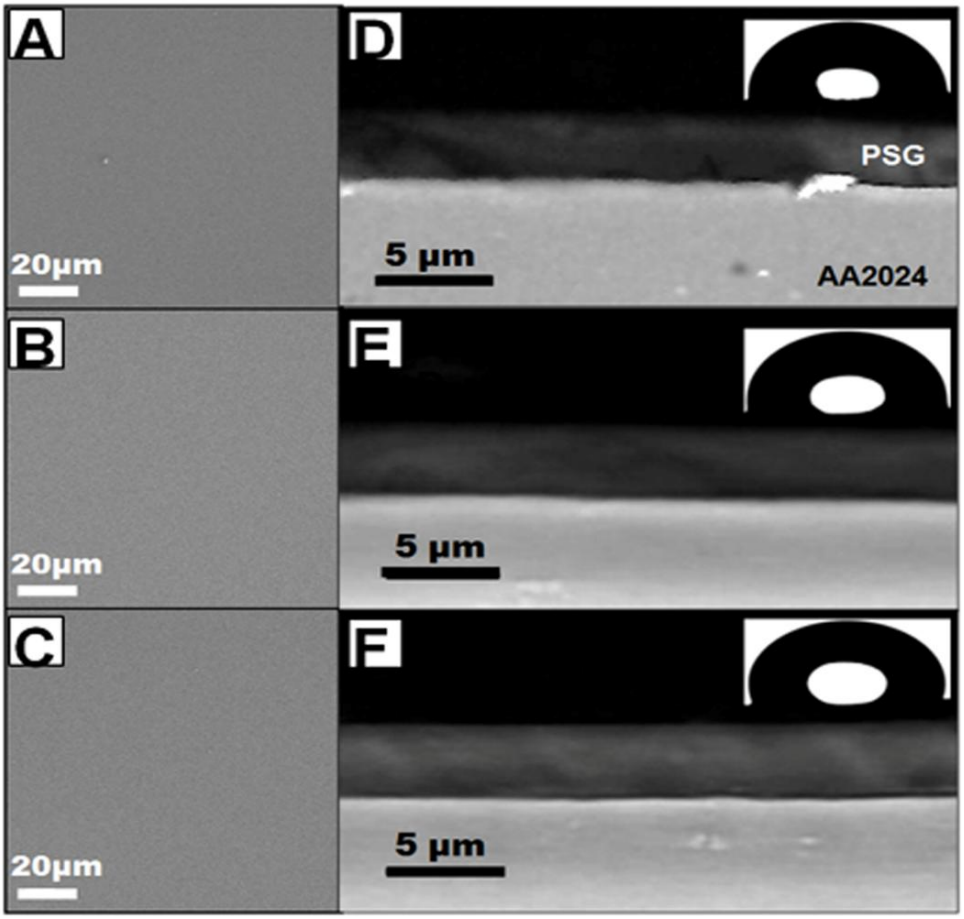

Figure 2. Scanning electron micrographs of the surfaces and cross-sections of the differently coated AA2024-T3 aluminium alloy: (a), (d) PSG-03; (b), (e) PSG-05; (c), (f) PSG-08. The inserts show a water drop placed on the differently coated AA2024-T3 aluminium alloy.

Figure 2 shows scanning electron micrographs of the surfaces and cross sections of the coated alloy before exposure to the testing media, revealing uniform coatings. From the cross sections of Figures 2 d, e and f, the coating thicknesses were determined and are presented in Table 1. The coating thicknesses follow the order: PSG-03 < PSG-05 < PSG-08. It is evident that the difference in polymer thicknesses depends on the structure of the polymeric matrix, associated mainly with the length of the aliphatic chain present in the precursors, as discussed later [26].

Table 1. Contact angle and thicknesses of the sol-gel coatings.

Sample	Contact angle (θ, °)	Thickness (μm)
Uncoated	67,6 ± 3,1	N.A.
PSG-03	91,1 ± 2,7	3,8 ± 1,7
PSG-05	96,5 ± 2,5	4,0 ± 1,5
PSG-08	104,4 ± 3,0	4,5 ± 1,3

Given that the bacterial micro-organisms are, by definition, hydrophilic systems and, consequently, have a better interaction with hydrophilic substrates, it is essential to know the hydrophobicity of the polymer systems. The inserts in Figure 2 display images of the water drop placed on the polymer surfaces, with the contact angles presented in Table 1. Although the contact angle values of the differently coated AA2024-T3 alloy surface suggested hydrophobic natures of the coatings, the values are not sufficiently high to confer to hydrophobic properties to the resulting antimicrobial capacity of the coatings [27-28].

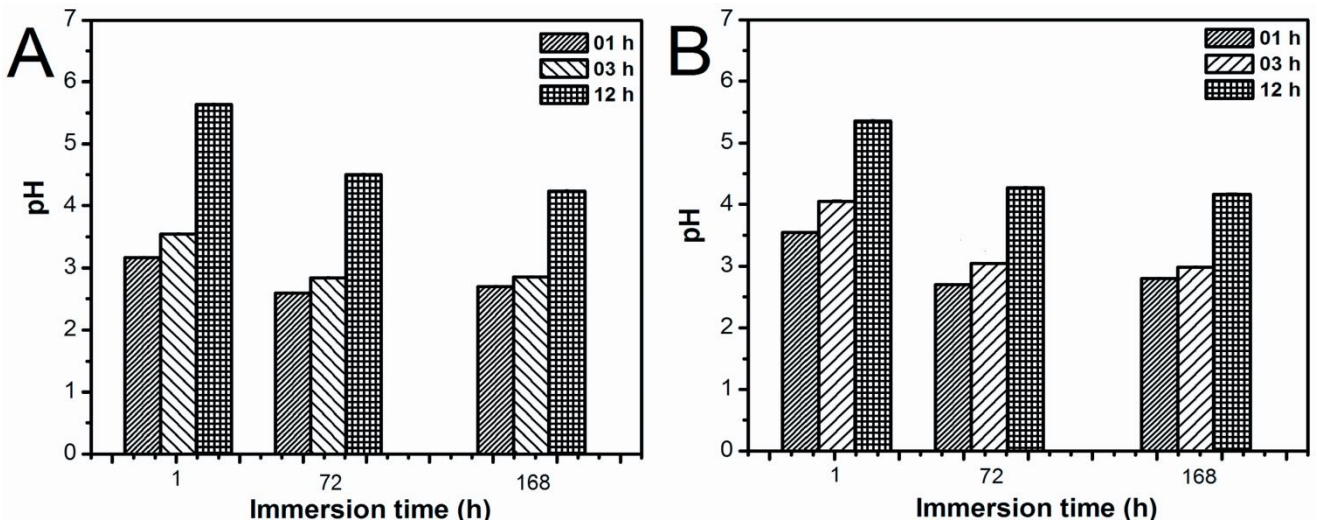

Figure 3. pH of the distilled water after the immersion of polymers that were cured for 1 h, 3 h and 12 h: (a) PSG-03; (b) PSG-08.

In order to understand the antibacterial properties of the hybrid polymers, and knowing that biofilm formation is susceptible to the acidity of the environment [35], pH variations of the distilled water that is in contact with the polymer were determined. The testing was conducted separately for two polymers, PSG-03 and PSG-08, with the results shown in Figure 3. It was revealed that through release of protons, a pH decrease was promoted in distilled water after immersion of the polymers in the water. The pH values of the water in the presence of PSG-08 polymer were approximately 10% higher than that in the presence of polymer PSG-03. This difference might be associated with the differences in porosity of the films, related to the degree of crosslinking of the aliphatic chains during

polymerization. Interestingly, the curing time influenced the change of pH. For the two polymers, the pH values of the water were higher after immersion of the polymers with a curing time of 12 h compared with other curing times. This suggests that the pH changes in the water are associated with the amount of occluded solvent in the polymer matrix. The solvent, which is associated with dissolved nitric acid (reaction catalyst), could be the source of protons during immersion of the polymers in distilled water.

3.2 Antibacterial properties

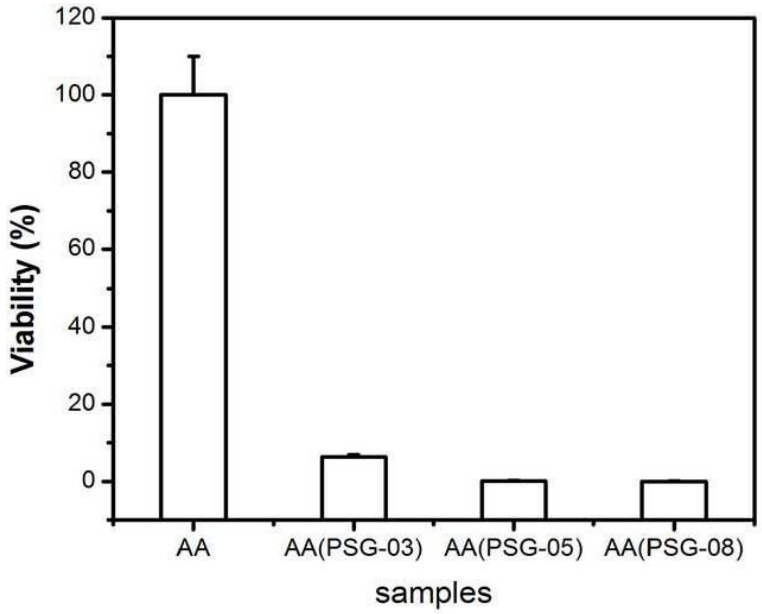

Figure 4. Percentage viability of *Pseudomonas aeruginosa* on the uncoated AA2024-T3 aluminium alloy and the alloy coated with PSG-03, PSG-05 and PSG- 08, after exposure to a media inoculated with *P. aeruginosa* for 16 h

The antibacterial properties of the coatings on the aluminium alloy were investigated following the Zapata procedure (described in Section 2.4), by comparing the viable cell numbers of *P. aeruginosa* on the uncoated and coated AA 2024 alloy samples after exposure to *P. aeruginosa* for 16 h. The results are summarized in Figure 4. It is evident that the polymers exhibit antibacterial activity against *P. aeruginosa*. The increased antibacterial capacity of polymer PSG-08 is perhaps related to the organic component, particularly to the length of the carbon chain present in the precursors, which was found to influence the hydrophobic properties of the resultant polymer. However, as discussed later, the antibacterial capacity could be also associated with the polymer structure and its ability to occlude solvent.

The bacterial viability of *P. aeruginosa* on the uncoated and coated AA2024 alloy samples was also assessed by confocal microscopy, after exposure to the bacterial strain (~ 10^8 CFU/ml) for 3 and 21 days. This was undertaken to determine the antibacterial ability of the polymer surfaces in the long term. The distributions of live and dead bacteria on the uncoated and coated substrates were

investigated using the fluorescent markers PI and SYTO 9, with dead cells displayed in red and live cells in green.

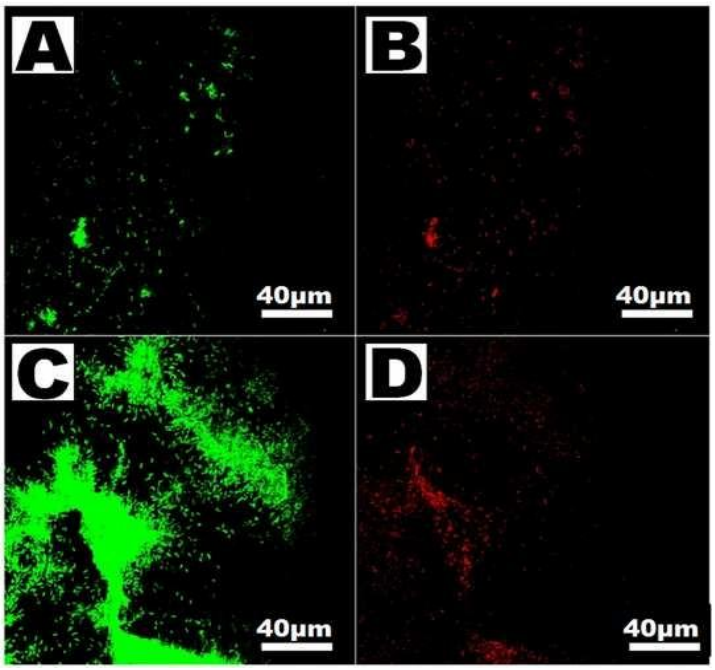

Figure 5. Fluorescence images of AA2024-T3 alloy surfaces under a green filter ((a),(c)) and a red filter ((b),(d)) after exposure to a media inoculated with *P. aeruginosa* for ((a),(b)) 3 days and ((c),(d)) 21 days.

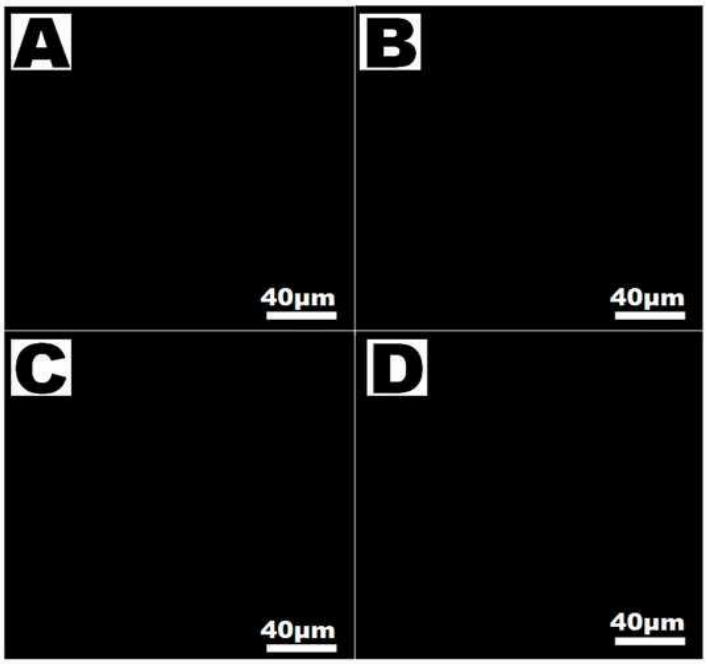

Figure 6. Fluorescence images of AA2024-T3 alloy coated with PSSG-08 under a green filter ((a),(c)) and a red filter ((b),(d)) after exposure to a media inoculated with *P. aeruginosa* for ((a),(b)) 3 days and ((c),(d)) 21 days.

For the uncoated AA2024-T3 alloy samples, Figure 5 shows representative images after exposure to the bacterial strain. The bacterial growth with exposure time reveals cellular clusters associated with the formation of biofilms. In contrast, for the coated AA2024 alloy, the fluorescent viability staining shows a dramatic reduction of bacterial presence, particularly for the alloy coated with polymer PSG-08 (Fig. 6), which revealed a complete absence of bacteria. As stated previously, the antibacterial ability of the polymers is probably multifactorial, which is discussed later.

3.5 Corrosion behaviour

Figure 7 shows scanning electron micrographs of the differently coated AA2024-T3 alloy samples after exposure to a media inoculated with *P. aeruginosa* for 3 and 21 days. The dark stripes revealed are associated with cracks. The widths of the dark stripes increased with exposure time to the culture broth. This may be the result of chemical ageing caused by moisture and the temperature during exposure to the culture medium in the presence of bacteria at 37°C [30-31].

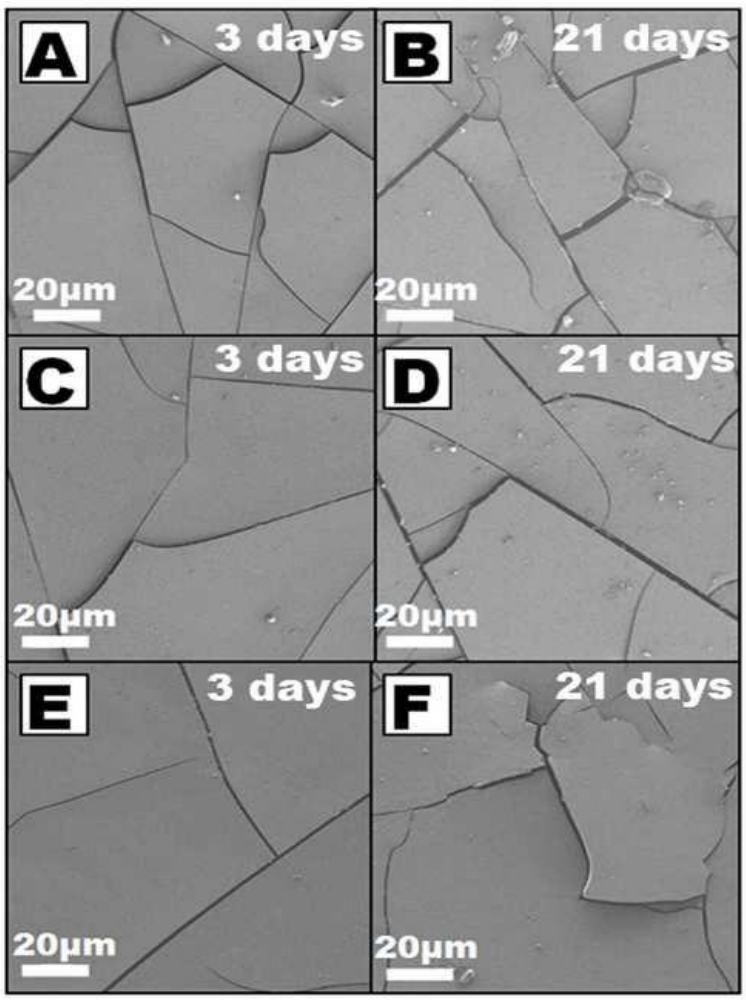

Figure 7. Scanning electron micrographs showing the surface morphology of the differently coated AA-2024 alloy after different exposure times to a media inoculated with *P. aeruginosa*: (a, b) PSG-03; (c, d) PSG-05; (e, f) PSG-08.

Figure 8 (a) shows a scanning electron micrograph of the uncoated AA2024 alloy surface after exposure to a media inoculated with *P. Aeruginosa* for 3 days. Localized corrosion is evident. EDX analysis of the localized corrosion sites detected relatively high level of copper, manganese and iron, as shown in Figure 8 (b), suggesting the presence of Al-Fe-Mn-Cu intermetallic particles at the sites. Thus, the bacteria influenced localized corrosion occurred preferentially at regions where Al-Fe-Mn-Cu intermetallic particles are present.

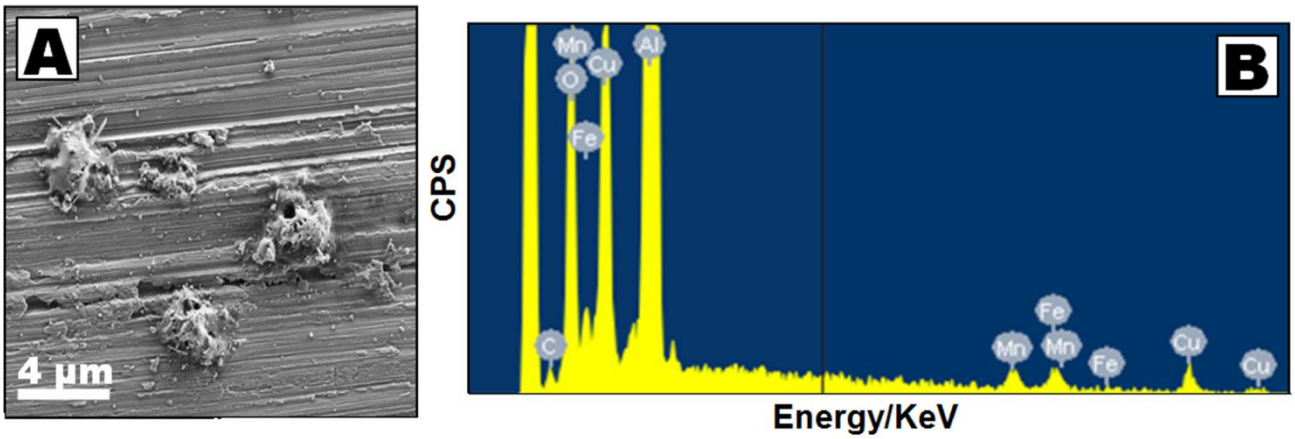

Figure 8. (a) Scanning electron micrograph of the uncoated AA2024 alloy surface after exposure to a media inoculated with *P. aeruginosa* for 3 days and (b) EDX spectrum of the corrosion sites

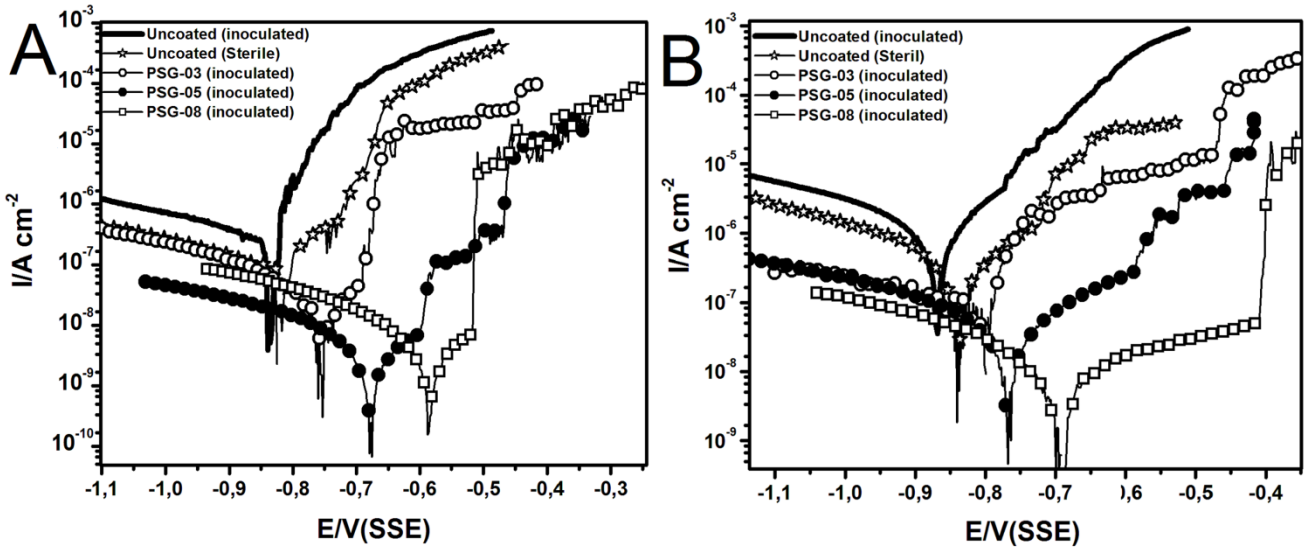

Figure 9. Potentiodynamic polarization curves of the uncoated and differently coated AA2024-T3 alloy in sterile medium, after exposure to a media inoculated with *P. aeruginosa* for (A) 3 days and (B) 7 days.

Figures 9 and 10 show the polarization curves of the uncoated and differently coated AA2024-T3 alloy samples in sterile medium, after the samples had been exposed to a culture medium

inoculated with *P. aeruginosa* for different time periods. The results are summarized in Table 2. From comparison of the E-I responses of the uncoated samples obtained in sterile media and sterile media inoculated with the bacteria (Fig.9), it is evident that the corrosion current is higher for the latter, suggesting an influence of *P. aeruginosa* on the alloy susceptibility to corrosion.

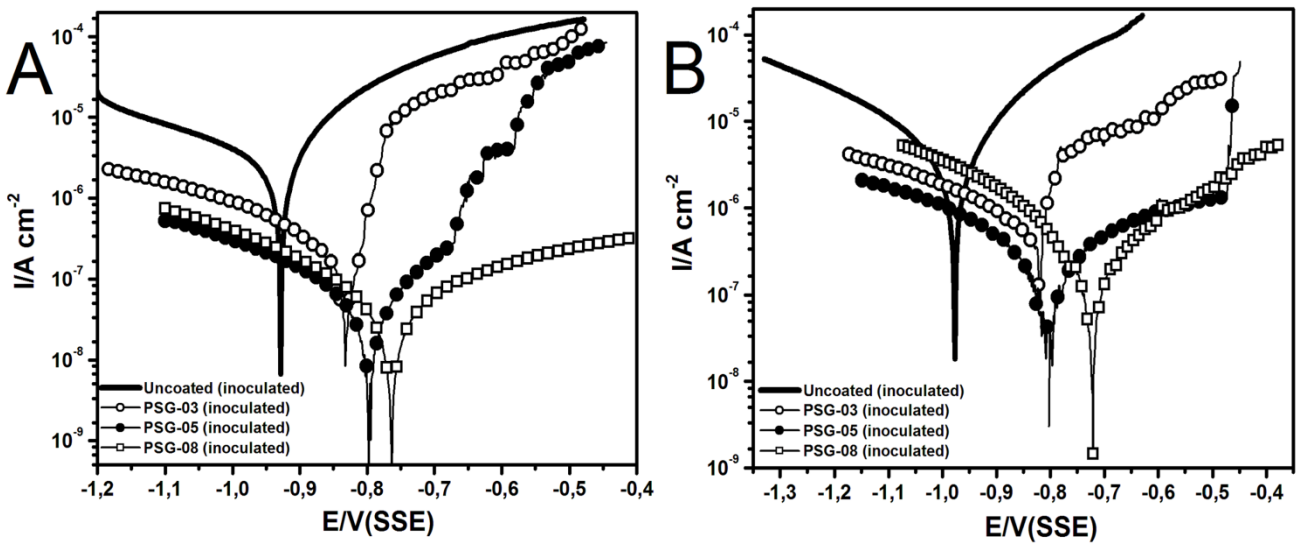

Figure 10. Potentiodynamic polarization curves of the uncoated and differently coated AA2024-T3 alloy in sterile medium, after exposure to a media inoculated with *P. aeruginosa* for (A) 14 days and (B) 21 days.

For the coated samples, to obtain the relative protection conferred by the different polymers, the protection efficiency (PE) was calculated using the following equation [32-33].

$$PE = \frac{I_0 - I_{corr}}{I_0}$$

where I_0 and I_{corr} represent the corrosion current densities of the uncoated and coated samples respectively. The PE values are listed in Table 2. It is evident that the corrosion potentials (E_{corr}) of the coated samples are more positive than that of the uncoated sample. This trend is commonly observed in metallic specimens that have been protected with sol-gel hybrid polymers [18] and it is associated with barrier-type characteristics provided by the polymer, which hinders access of electrolyte to the metal-polymer interface. For the differently coated samples, the corrosion potential increases in the following order PSG-03 < PSG-05 < PSG-08, which reflects the coating thicknesses (Figs. 2 d, e and f).

A further feature of the coated specimens is the change of corrosion potential with increasing time of exposure to the bacterial culture, which shifts in the negative direction for all coatings, and also a progressive increase in the corrosion current. This indicates that the increased period of contact between the coating and bacterial culture increased the susceptibility to corrosion. Despite the gradual increase of the corrosion current with the exposure time, even after 21 days the coated samples

exhibited corrosion current densities two orders of magnitude lower than those of the uncoated alloy. Thus, the corrosion and biocorrosion resistances of the coatings remained after exposure to the corrosive media for extended periods of time, suggesting that the cracks revealed in Fig.7 are not deep. Based on the current density values in Table 2, the best protection efficiency (PE) was exhibited after 7 days of exposure, with the following order revealed: PSG-03 < PSG-05 < PSG-08. It is further noted that the I_{corr} values of the alloy coated with the various polymers increased with the time of exposure to the bacterial strain, indicating a progressive deterioration of the coatings with exposure time. However, the barrier property was retained to a degree even after 14 days exposure since the I_{corr} values remained below the values of the uncoated specimens.

Table 2. Corrosion parameters calculated from Figs 9 and 10

Exposure time (days)	AA-2024		AA-2024 (PSG-03)		AA-2024 (PSG-05)		AA-2024 (PSG-08)	
	E_{corr} (V)	I_{corr} (A cm^{-2})	E_{corr} (V)	I_{corr} (A cm^{-2})	E_{corr} (V)	I_{corr} (A cm^{-2})	E_{corr} (V)	I_{corr} (A cm^{-2})
3	-0.834	$2.1X10^{-7}$	-0.758	$1.8X10^{-8}$	-0.674	$2.0X10^{-9}$	-0.585	$2.2X10^{-9}$
7	-0.871	$4.9X10^{-7}$	-0.799	$7.7X10^{-8}$	-0.769	$2.0X10^{-8}$	-0.694	$3.9X10^{-9}$
14	-0.928	$2.1X10^{-6}$	-0.833	$1.1X10^{-7}$	-0.795	$2.5X10^{-8}$	-0.762	$1.6X10^{-8}$
21	-0.979	$2.5X10^{-6}$	-0.821	$3.9X10^{-7}$	-0.798	$1.3X10^{-7}$	-0.723	$1.2X10^{-7}$

4. DISCUSSION

4.1 Coating charaterization.

Figure 1 enables comparison between the signal intensities of the different polymers in the region 2600-3100 cm^{-1}, which show the absorbances corresponding to the symmetrical stretching of -CH_2. The intensities for the polymers PSG-03, PSG-05 and PSG-08 give the ratios of 2:4.1:7.3. This confirms that the main difference between the polymers is the aliphatic chain length of one of the substituents on the second precursor. Relating this information to the various coating thicknesses (Figs. 2 d, e and f), it is evident that the longer the aliphatic chain, the greater the coating thickness. In similar studies related to the protection of aluminium alloys with silanol-type polymers, Metroke et al [26] reported a relationship between the coating thickness and the presence of organic substituents in the precursors. The coating thickness was higher when the contribution of the organic substituent in the silanols was higher. Moreover, using FT-IR to monitor the process of gelation of the following systems, TEOS and TEOS-PAMS (tetraethylsilane phenylaminomethyltrietoxysilane), differences in gelation times were revealed. For TEOS, the gelation time was 145 h and for the TEOS-PAMS system (in the ratio 6.5:1) the gelation time was ~ 5 h [25]. The differences in gelation times have been associated with the different reaction rates of both the hydrolysis and the condensation reactions. For the TEOS-PAMS systems, the reaction rate of hydrolysis is lower, while the condensation reaction is increased. This can be linked to (a) steric hindrance provided by the organic substituent and (b) the

increase in pH values. It is possible that in the case of the PSG-08, PSG-05 and PSG-03 polymers, the differences in the thickness achieved are the result of differences in the kinetics of the hydrolysis and condensation reactions. These are also connected with the steric hindrance resulting from the extension of the aliphatic chain of one substituent in the precursor.

4.2 Antibacterial properties

Viability tests (Fig. 4) and fluorescence confocal microscopy (Figs. 5-6) showed that the polymers possess antibacterial property against *P. aeruginosa*. The antibacterial capacity of the polymers followed the order: PSG-08 > PSG-05 > PSG-03. This suggests that there is a correspondence between the structure of the polymer matrix and the antibacterial property, which could be associated with the hydrophobic properties of the polymer films. The contact angle measurements confirmed that there are differences in hydrophobicity between the polymers, which follow the order: PSG-08 > PSG-05 > PSG-03. However, as mentioned in the Results Section, the contact angle values are not sufficiently high to confer to hydrophobic properties to the antimicrobial capacity of the coatings. According to Vilenik et al [27], when the contact angle is equal to or greater than 140°, hydrophobicity ensures sufficient capacity to prevent biofilm formation in *Escherichia coli*.

Considering the above, and knowing that the variation in pH may also affect bacterial viability on the polymer surfaces, the pH variation of distilled water that is in contact with the polymers was studied. The results showed that the pH decreased with the immersion time of the polymer in the water (Fig. 3). Further, the experiments performed for the polymers with different curing times revealed that the changes in pH were less significant with polymers that were cured for longer time. This suggests that the change in pH could be associated with solvent occluded in the polymer matrix, which is expected to present a low pH associated with the acid catalyst (nitric acid) used in the hydrolysis and condensation processes for the generation of the polymers. The results agree with similar studies reported in the literature. For example, the reduction of the bacterial viability over the sol-gel polymer surfaces against *E.coli*, which remains latent even after 550 days of storage at 4°C and 20°C, has been explained by occlusion of acid solvent in the polymer matrix, where the acidity of the solvent has been linked to the use of HCl as catalyst [34]. Further, Hostaká et al [35] examined the effect of pH on biofilm development in *P. aeruginosa* bacteria (6819). This study demonstrated that the formation of the biofilm at pH 7.5 is 164% higher than at pH 5.5. The authors suggested that the production of alginate (polysaccharide), the main component of the biofilm skeleton, was diminished by the decrease of pH.

4.3 Corrosion behaviour

The surface morphology of the uncoated samples shows that AA2024 alloy markedly deteriorates with time of exposure to the bacterial culture (Fig 8). In addition, EDX analysis revealed that the surface damage is related to the presence of local high copper contents an also to the presence of Fe and Mn [36-38]. Similar results have been reported for prolonged exposure of AA2024 alloy to

Serratia marcescens and *Bacillus cereus* bacteria [39]. For these type of bacteria, it is suggested that the biocorrosion process is driven by the formation of a biofilm and the presence of the catalase enzyme, which is excreted during the bacteria metabolism. The enzyme, which overcomes the toxic nature of hydrogen peroxide by breaking it down into water and oxygen, reduces the oxygen content within the biofilm. Similar results have been reported for *E.coli* on stainless steel [40]. The oxygen radical produced during the bacterial metabolism binds to the aluminium atom present on the alloy surface and forms a superoxide surface anion radical. Further, it was suggested that the ability of the bacteria to oxidize aluminium and to form a low-density aluminium hydroxide and $AlCl_3$ in the corrosion tubercles is the key factor of pitting corrosion of the alloy [40]. Reactions associated with respiration and metabolism of microorganisms make the system much more complex to analyze and has motivated additional studies, which are currently in progress.

The electrochemical measurements (Figs. 9 and10) showed that the polymers provided protection for the AA2024 alloy, even after long periods of exposure to the culture medium. The difference in protection efficiency of the three types solgel coatings, we associate it with the difference in the long aliphatic chain, which affects the degree of crosslinking during polymerization. The long chain aliphatic promote greater crosslinking during polymerization, and thus, obtaining polymer thicker, more compact and more hydrophobic [25]. However, this explains only antifouling properties of the three polymers against *P. aeruginosa*, but not, bactericidal capacity observed. Considering the results shown in Table 1 and Figure 3, we believe that the antibacterial property could be attributed to the synergistic effect between the hydrophobic properties of polymers, and the pH changes occurring in the polymer-electrolyte interface. Although the occurrence of cracks in the coatings was evident with prolonged exposure of the coated samples in the culture media, the comparison of the corrosion current of the uncoated samples with those coated showed clearly that the protection was retained.

5. CONCLUSIONS

The hybrid coatings, TEOS/TEOCS, TEOS/TEPRS and TEOS/TEPES, showed remarkable antibacterial ability against *P. aeruginosa*, which is attributed to a synergistic effect between two factors, namely the hydrophobicity of the polymer film and the ability of the polymeric matrix to release protons, which promotes pH changes at the polymer-electrolyte interface. Electrochemical measurements revealed the ability of the coatings to protect the aluminium alloy from biocorrosion in media inoculated with the bacterium *P. aeruginosa*. Further, a correlation between the degree of protection and the length of the aliphatic chain was found. The longer the chain length, the greater the protective effect.

ACKNOWLEDGMENTS

This work was supported by FONDECYT (Grants Nº 1100537) and PIA (ACT 95). M.A. Páez and M. I. Azócar are also grateful to CONICYT (Grant 79090024). The authors also wish to thank the UK Engineering and Physical Sciences Research Council for provision of financial support for the LATEST2 Programme Grant.

References

1. J. W. Costerton, P. S. Stewart, E. P. Greenberg, *Science*, 284 (1999) 1318.
2. I. B. Beech, *Int. Biodeter*. 53 (2004) 177-183.
3. A. Rajasekar, S. Maruthamuthu, N. Muthukumar, S. Mohanan, P. Subramanian and N. Paraniswamy,*Corros. Sci*. 47 (2005) 257-271.
4. I. B. Beech and J. Sunner, *Curr. Opi. Biotechnol*. 15 (2004) 181-186.
5. A. Rajasekar and Y. P. Ting, *Ind. Eng. Chem. Res*. 50 (2011) 12534-12541.
6. S. J. Yuan, A. M. Choong, S. O. Pehkonen, *Corros. Sci*. 49 (2007) 4352-4385.
7. R. Armon, J. Starosvetsky, M. Dancygier and D. Starosvetsky, *Biofouling*, 17 (2001) 289-301.
8. V. F. Smirnov, D. V. Belov, T. N. Sokolova, O. V. Kuzina and V. R. Kartashov, *Appl. Biochem. Microbiol.* 44 (2008) 192-196.
9. M. J. Vieira, R. Oliveira, L. Melo, M. M. Pinheiro, V. Martins, *Colloid. Surface.* B. 1 (1993) 119-124.
10. A. Abbas, N. Parviz, G. M. Reza, *J. Biotech*. 136 (2008) S619
11. H. G. Hedrick, C. E. Miller, J. E. Halkias and J. E. Hildebrand, *Appl. Environ. Microbiol*. 12 (1964) 197.
12. A. Hagenauer, R. Hilpert, T. Hack, *Mater. Corros*. 45 (1994) 355-360.
13. S. V. Lamaka, D. G. Shchukin, D. V. Andreeva, M. L. Zheludkevich, H. Möhwald, M. G. Ferreira, *Adv. Funct. Mater*. 18 (2008) 3137–3147.
14. S. V. Lamaka, M. F. Montemor, A. F. Galio, M. L Zheludkevich, C. Trindade, L. F Dick, M. G., *Electrochim. Acta*, 53 (2008) 4773–4783.
15. M. L. Zheludkevich, I. M. Salvado, M. G., *J. Mater. Chem*. 15 (2005) 5099–5111.
16. G. Schottner, *Chem. Mater*. 13 (2001) 3422-3435.
17. U. Sanchez, G. J. Soler-Illa F. Ribot, C. R. Mayer, V. Cabuil, T. Lalot, *Chem. Mater*.13 (2001) 3061–3083.
18. E. Gonzalez, J. Pavez, I. Azocar, J. H. Zagal, X. Zhou, F. Melo, G. E. Thompson, M. A. Páez, *Electrochim. Acta*. 56 (2011) 7586-7595.
19. A.W. Bauer, W.M.M. Kirby, J.C. Sherris, M. Turck, *Am. J. Clin. Pathol*. 45 (1966) 493–496.
20. P. A. Zapata, L. Tamayo, M. Páez, E. Cerda, M. I. Azócar, F. M. Rabagliati, *Eur. Polym. J.* 2011
21. M. S. Gião, S. A. Wilks, N. F. Azevedo, M. J. Vieira & C. W. Keevil, *Microb. Ecol.*, 58 (2009), 56–62.
22. J. Gallardo, A. Durán, D. Di Martino, R. M. Almeida, *J. Non-Cryst. Solids*, 298 (2002) 219–225.
23. P. Innocenzi, *J. Non-Cryst. Solids*. 316 (2003), 309–319
24. H. Jeon, S. Yi, S. Oh, *Biomaterials*. 24 (2003) 4921–4928.
25. C. Wu, Y. Wu, T. Xu, and W. Yang, *J. Non-Cryst. Solids*., 352 (2006) 5642–5651.
26. T. L. Metroke, J. S. Gandhi and A. Apblett, *Prog. Org. Coat*. 50 (2004) 231-246.
27. A. Vilenik, I. Jerman, A. Vuk, M. Kozelj, B. Orel, B. Tomisic, B. Simoncic, and J. Kovac, *Langmuir*. 25 (2009), 5869–5880.
28. N. P. Boks, W. Norde, H. C. van der Mei and H. J. Busscher, *Microbiology*. 154 (2008), 3122–3133.
29. J. Yuan, S. Pehkonen, Y. Ting, K Neoh, E. Kang, *Langmuir*. 26 (2010) 6728-6736
30. K. Hiromitsu, K. Masahiro, H. Toshihiro and K. Katsumi, *J. Sol-Gel Sci. Techn*. 19 (2000) 205-209.
31. W. Duhua, P. Gordon, *Prog. Org. Coat*. 64 (2009) 327-338.
32. S. J. Yuan, S. O. Pehkonen, Y. P. Ting, K. G. Neoh, E. T. Kang, *Appl. Mater. Interfaces*. 1 (2009) 640–652.
33. G. J. Copello, S Teves, J. Degrossi, M. D´Aquino, M. F. Desimone and L. E. Diaz, *J. Ind. Microbiol. Biot.* (2006) 343-348.

34. G. S. Alvarez, M. L. Foglia, G. J. Copello, M. F. Desimone and L. E. Diaz, *Appl. Microbiol. Biotechnol.* 82 (2009) 639–646.
35. A. Hostaká, I. Ciznár, M. Stekovicová, *Folia microbiol*. 55 (2010) 77-78.
36. A. Boag, A.M. Glenn, D. McCulloch, T.H. Muster, C. Ryan, C. Luo, X. Zhou, G.E. Thompson and A.E. Hughes, *Corros. Sci*. 53 (2011) 27-39
37. A.M. Glenn, T.H. Muster, C. Luo, X. Zhou, G.E. Thompson, A. Boag and A.E. Hughes, *Corros. Sci.*, 53 (2011) 40-50.
38. X. Zhou, C. Luo, T. Hashimoto, A.E. Hughes, G.E. Thompson, *Corros. Sci*. 58 (2012) 299-306.
39. A. Rajasekar and Y. Ting, *Ind. Eng. Chem. Res*. 49 (2010) 6054-6061.
40. S.Baeza, N.Vejar, M.Gulppi, M.Azocar, F.Melo, A.Monsalve, J.Pérez-Donoso, C.C.Vásquez, J.Pavez, J.H.Zagal, X.Zhou, G.E.Thompson and M.A.Páez, *Corros. Sci*. 67 (2013) 32-41.